Analytica Chimica Acta 768 (2013) 69–75

Contents lists available at SciVerse ScienceDirect

Analytica Chimica Acta

journal homepage: www.elsevier.com/locate/aca

Preparation of cobalt-tetraphenylporphyrin/reduced graphene oxide nanocomposite and its application on hydrogen peroxide biosensor

Longzhen Zheng*, Dan Ye, Leyan Xiong, Jingpeng Xu, Kun Tao, Zhijun Zou, Danlin Huang, Xiaowei Kang, Shaoming Yang, Jian Xia

Department of Chemistry and Chemical Engineering, East China Jiao Tong University, Nanchang, Jiangxi 330013, PR China

HIGHLIGHTS

- CoTPP/RGO nanocomposite was prepared by a π–π stacking interaction.
- CoTPP/RGO showed electrocatalytic activity for both oxidation and reduction of H_2O_2.
- The high sensitivity was due to the synergy effect between CoTPP and RGO.
- The CoTPP/RGO electrode showed good anti-interfering ability.

GRAPHICAL ABSTRACT

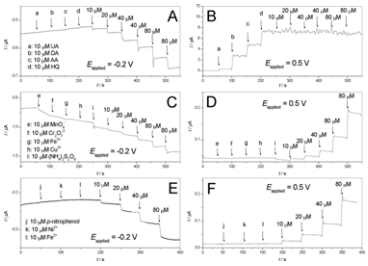

ARTICLE INFO

Article history:
Received 2 December 2012
Received in revised form 8 January 2013
Accepted 12 January 2013
Available online 21 January 2013

Keywords:
Cobalt-tetraphenylporphyrin
Reduced graphene oxide
Nanocomposite
Hydrogen peroxide biosensor
Anti-interfering ability

ABSTRACT

A novel cobalt-tetraphenylporphyrin/reduced graphene oxide (CoTPP/RGO) nanocomposite was prepared by a π–π stacking interaction and characterized by ultraviolet–visible absorption spectroscopy (UV–vis), Fourier transform infrared spectroscopy (FTIR) and electrochemical impedance spectroscopy (EIS). The CoTPP/RGO nanocomposite exhibited high electrocatalytic activity both for oxidation and reduction of H_2O_2. The current response was linear to H_2O_2 concentration with the concentration range from 1.0×10^{-7} to 2.4×10^{-3} mol L^{-1} ($R = 0.998$) at the reductive potential of −0.20 V and from 1.0×10^{-7} to 4.6×10^{-4} mol L^{-1} ($R = 0.996$) at the oxidative potential of +0.50 V. The H_2O_2 biosensor showed good anti-interfering ability towards oxidative interferences at the oxidative potential of +0.50 V and good anti-interfering ability towards reductive interferences at the reductive potential of −0.20 V.

1. Introduction

Porphyrin is a kind of macrocyclic conjugated organic molecules which has an extensive system of delocalized π-electrons. The porphyrin can coordinate with many metal ions (such as Fe, Co, Cu, and Zn) to form stable metal–porphyrin coordination complexes, which are widely existed in nature with special physiological activity and excellent properties in electron transfer, energy conversion, and nonlinear optical-limiting [1–3]. As the mimics of the active site of many important enzymes, porphyrins have been used as electron media with good electrocatalysis toward reduction or oxidation of many small molecules related to life process [4]. They are extensively studied for the functionalization of carbon nanotubes (CNTs) by both covalent and non-covalent methods [5–7]. Compared with covalent functionalization, non-covalent functionalization of porphyrin has the advantage of simple, convenient, avoiding destruction of the structure of some polycyclic and unstable substance and preserving their unique properties without serious damage.

Graphene (GR), a new class of two-dimensional carbon nanostructure, has been extensively studied recently in terms of high conductivity, large surface-to-volume ratio and superior chemical and mechanical stability. It has been widely used in nanoelectronics, batteries, supercapacitors and solar cells [8–11]. Considering

* Corresponding author. Tel.: +86 791 87046351; fax: +86 791 87046320.
E-mail address: zlz@ecjtu.jx.cn (L. Zheng).

0003-2670/$ – see front matter © 2013 Elsevier B.V. All rights reserved.
http://dx.doi.org/10.1016/j.aca.2013.01.019

its two-dimensional structure, graphene could be used as excellent substrate for the assembly of porphyrins. Recently, graphene hybrid materials functionalized with different porphyrin derivatives have been well studied [12–15].

In the present manuscript, cobalt-tetraphenylporphyrin (CoTPP) molecules were assembled on the surface of reduced graphene oxide (RGO). Metal–porphyrin molecules were flattened on the surface of RGO through non-covalent π–π stacking interaction and the conjugation of metal–porphyrin is enlarged. The flattening of metal–porphyrin molecules can further reduce the distance between the metal–porphyrin planes and RGO, which further enhance π–π stacking interaction. The CoTPP/RGO nanocomposite showed high electrocatalytic activity both for oxidation and reduction of H_2O_2. The CoTPP/RGO nanocomposite can be a good candidate for the electrochemical detection of H_2O_2 with high sensitivity and selectivity.

2. Experimental

2.1. Reagents

Graphite and tetra-phenylporphyrin (TPP) were purchased from Sigma–Aldrich. Hydrogen peroxide (30%), hydrazine (50%), $CoCl_2$, and other chemicals were of analytical grade and purchased from Beijing Chemical Reagent Co. (Beijing, China). All solutions were made up with twice-distilled water.

2.2. Apparatus and measurements

The UV–vis absorption spectra were recorded on a Lambda 35 UV/VIS Spectrometer (PerkinElmer Precisely, USA).

FTIR spectra were conducted on a Spectrum One FTIR Spectrometer (PerkinElmer Instruments, USA) and transmission spectrum of the samples were obtained by forming thin transparent KBr pellet.

Atomic force microscopy (AFM) images were revealed by a AFM AJ-III (Aijian, Shanghai).

Electrochemical impedance spectra (EIS) measurements were conducted by a Solartron 1255B frequency response analyzer combined with a Solartron 1286 electrochemical interface (Solartron Farnborough, UK). An IEEE-interface (National Instruments, USA) was employed to couple the two Solartron instruments with a computer.

Electrochemical measurements were performed on a CHI 660A electrochemical workstation (Chenhua, China) with a conventional three-electrode system with the modified glassy carbon electrode GCE (Φ = 5 mm) as working electrode, a platinum wire as auxiliary electrode, and an Ag/AgCl (saturated KCl) electrode as reference against which all potentials were measured.

2.3. Preparation of RGO and CoTPP complex

Graphene oxide (GO) was prepared from natural graphite flakes by a modified Hummer's method [16]. Briefly, graphite (3.0 g) was added to concentrated H_2SO_4 (70 mL) under stirring at room temperature. Then $NaNO_3$ (1.5 g) was added and the mixture was cooled to 0 °C. Under vigorous agitation, $KMnO_4$ (9.0 g) was added slowly to keep the temperature of the suspension lower than 20 °C. The mixture was stirred at 35 °C for 2 h. Then distilled water (150 mL) was added and the solution was stirred at 90 °C for 15 min. Additional 500 mL of distilled water was added and followed by a slow addition of 15 mL of H_2O_2 (3%), turning the color of the solution from dark brown to yellow. The mixture was filtered and washed with 1:10 HCl aqueous solution (250 mL) to remove metal ions followed by washing with 200 mL of distilled water to remove the acid. The resulting solid was dried in air and diluted to make a GO aqueous dispersion (0.5 wt%).

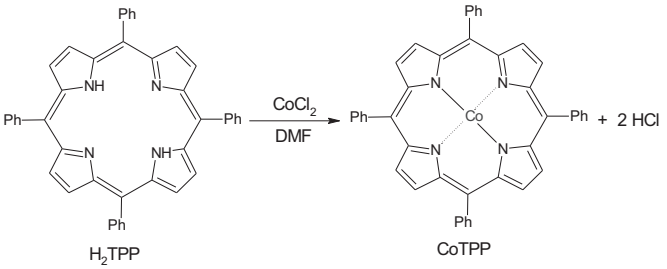

Scheme 1. Synthetic scheme of CoTPP.

RGO was prepared through the procedures reported by Li et al. [17]. Briefly, GO aqueous dispersion (50 mL) was mixed with hydrazine hydrate (0.1 mL, 50 wt%) and ammonia solution (0.5 mL, 28 wt%). The mixture was stirred at 95 °C for 1 h. After reduction, a homogeneous black dispersion with a small amount of black precipitate was obtained. The dispersion was filtered by glass cotton to remove the precipitate and a stable black aqueous dispersion of RGO was obtained.

CoTPP was prepared by a simple complexation reaction (Scheme 1). Briefly, TPP (3.07 g, 5 mmol) was dissolved in DMF (100 mL) and then $CoCl_2$ (0.65 g, 5 mmol) was added to the TPP/DMF solution. The mixture was stirred for 10 min at room temperature and then refluxed for 6 h. Then the DMF solvent was distilled under reduced pressure and the residue was poured into the cooling water. The product was collected, acidified with concentrated HCl, and then filtrated. Finally the CoTPP was washed with distilled water, dried over, and recrystallized with mixture solvent of dichloride methane and absolute ethanol.

2.4. Preparation of CoTPP/RGO modified electrode

Before modification, the bare GCE was polished with 0.3 μm and 0.05 μm alumina slurry, then washed successively with anhydrous ethanol and distilled water in an ultrasonic bath for 10 min and dried in N_2 blowing.

The CoTPP/RGO nanocomposite was prepared by π–π stacking interaction. First, RGO aqueous dispersion (0.25 mg mL^{-1}, 1 mL) was dropped into a CoTPP/DMF solution (5 μM, 1 mL) dropwise under vigorous stirring. After dropping, the mixed solution was treated by ultrasonic waves for 30 min for complete interaction between CoTPP and RGO. The CoTPP/RGO dispersion was filtrated and washed with absolute ethanol for 3 times and then dried at 60 °C for 4 h in a vacuum. Then, 0.2 mg CoTPP/RGO was dispersed in 1 mL DMF and then 10 μL Nafion solution (5%, Aldrich) was added and sonicated for 30 min. Finally, 5 μL CoTPP/RGO dispersion was casted on the freshly prepared GCE surface by a micropipette to form a thin layer and stored at 4 °C in a refrigerator before use.

For comparison, CoTPP modified electrode was prepared using the same method. 10 μL Nafion solution (5%, Aldrich) was added in 1 mL of 5 μM CoTPP/DMF solution and then sonicated for 30 min. Finally, 5 μL CoTPP solution was casted on the freshly prepared GCE surface by a micropipette to form a thin layer and stored at 4 °C in a refrigerator before use.

2.5. Measuring procedure

Cyclic voltammetric measurements were done in an unstirred electrochemical cell. Amperometric experiments were carried out by applying a potential step of −200 or 500 mV to a stirred electrochemical cell. Aliquots of a standard solution of H_2O_2 were successively added to the solution. Current–time data were recorded after a steady-state current was achieved. All

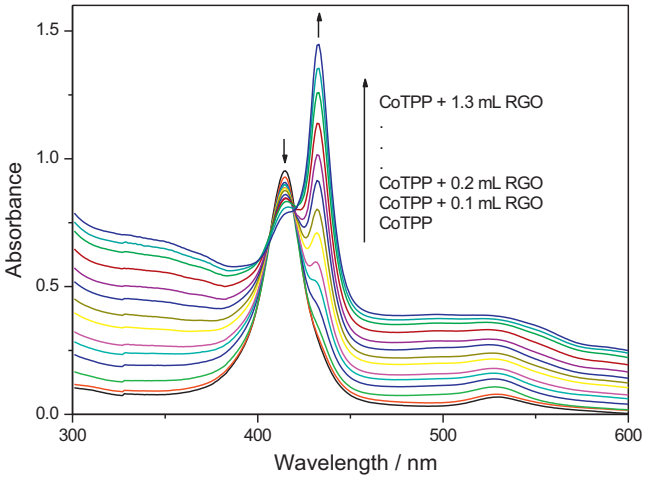

Fig. 1. UV absorption spectra recorded during the process of titration of 2 mL of 5 μM CoTPP DMF solution with various volumes of 0.25 mg mL^{-1} RGO dispersion.

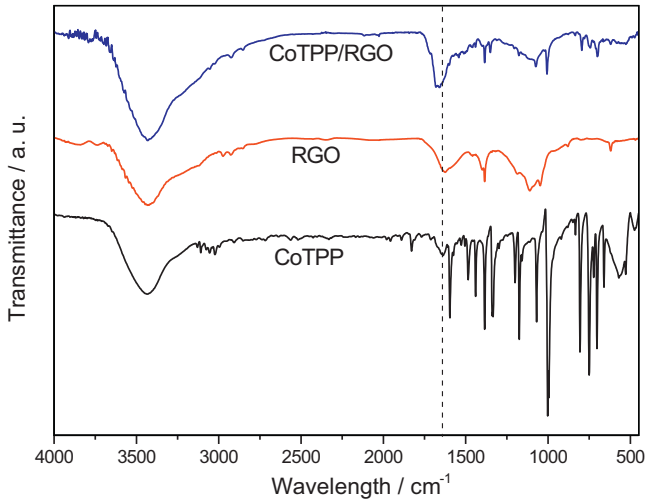

Fig. 2. FTIR spectra of CoTPP, RGO and CoTPP/RGO complex.

experimental solutions were deaerated by high pure nitrogen for 10 min, and a nitrogen atmosphere was kept over the solutions during measurements.

The impedance spectra were recorded using an AC perturbation signal of 5 mV within the frequency range of 10^6–0.01 Hz. The impedance data were fitted with an equivalent circuit using the *Z* plot/*Z* view software (Scribner Associates Inc., England). The equivalent circuit provided an electrical analogue of the chemical/physical processes probed by EIS. Impedance measurement was performed in the presence of a 1.0 mmol L^{-1} $K_3[Fe(CN)_6]/K_4[Fe(CN)_6]$ (1:1) mixture containing 1.0 mol L^{-1} KCl as a redox probe at the formal potential of the system.

3. Results and discussion

3.1. Characterization of CoTPP/RGO nanocomposite

The planar CoTPP molecule can be assembled onto the two-dimensional surface of RGO to form CoTPP/RGO nanocomposite through π–π stacking interaction. The interplay between CoTPP molecule and RGO during the process of assembly was studied by UV–vis spectroscopy. Fig. 1 showed the UV–vis spectra of CoTPP/DMF solutions titrated with different amounts of RGO dispersion. An intense Soret band at 415 nm was observed in the spectrum of CoTPP. During the titration process, the intensity of the original Soret band at 415 nm decreased gradually and a new Soret band at 433 nm appeared and intensified with an isosbestic

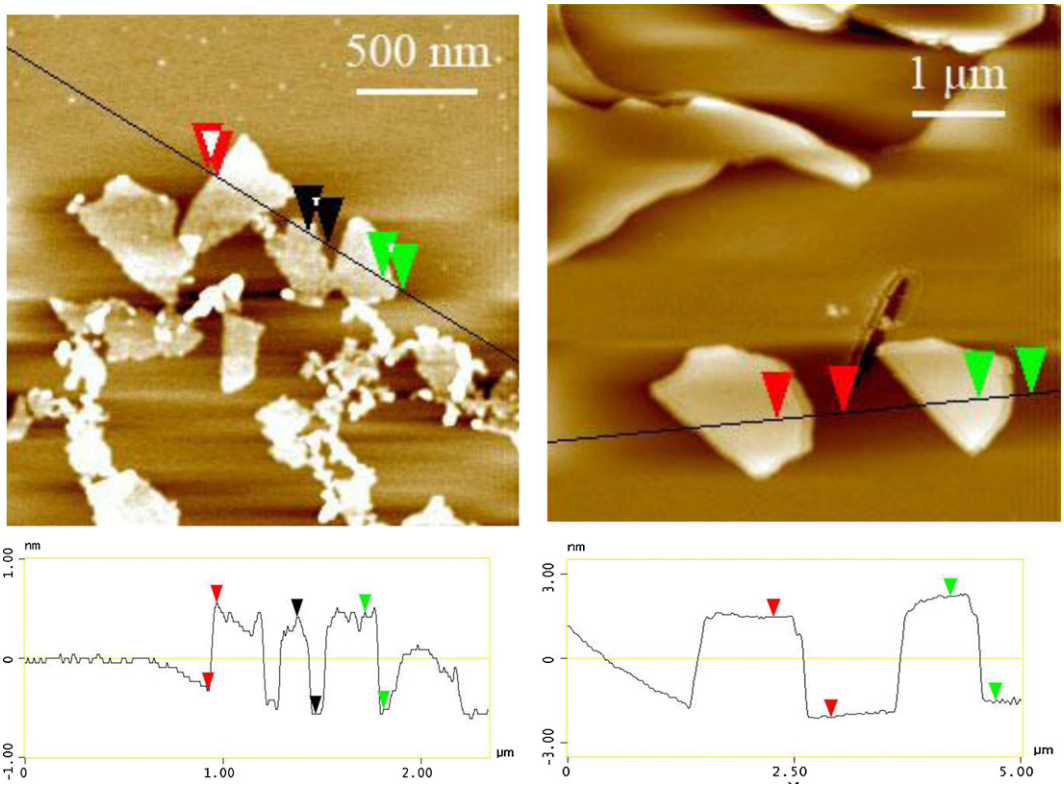

Fig. 3. AFM images of RGO (left) and CoTPP/RGO complex (right).

Table 1
Comparison of H_2O_2 sensor performance based on different electrode modified materials.

Modified material	Applied potential (V)	Linear range (μM)	Detection limit (μM)	Sensitivity (μA mM^{-1} cm^{-2})	Reference
CAT/nanoNiO/MWCNTs	Red: −0.45	200–2530	19	338	[18]
CS/Hb/AgNP	Red: −0.4	0.08–250	0.05	–	[19]
FeS/FTO	Red: −0.4	0.5–1300	0.12	2488	[20]
MnO_2/OMC	Ox: 0.45	0.5–600	0.07	807	[21]
Cu-Co alloy dendrite	Red: −0.4	1–11,000	0.75	1274	[22]
CuO/CPE	Ox: 0.60	0.05–1000	0.02	1746	[23]
FTS-PPy	Red: −0.73	10–4000	5	653	[24]
$LaNi_{0.6}Co_{0.4}O_3$	Ox: 0.55	0.01–100	0.001	1813	[25]
CoTPP/RGO	Ox: 0.50	0.1–460	0.02	6.6	Present
	Red: −0.20	0.1–2400	0.03	4.2	Present

point at 420 nm. A large bathochromic shift (18 nm), a narrower half-bandwidth, and stronger extinction of CoTPP/RGO dispersion were obtained compared with that of pure CoTPP solution. The phenomenon can be explained by molecular flattening mechanism. When CoTPP molecule was flattened on the surface of RGO with big π structure *via* π–π stacking interaction, the π conjugation effect of CoTPP will be enhanced. As a result, the Soret band of CoTPP showed a large bathochromic shift. So it can be concluded that CoTPP/RGO nanocomposite was formed with CoTPP molecule extensively adsorbed on the surface of RGO by simply mixing CoTPP solution and RGO dispersion together.

The FTIR spectra of CoTPP, RGO, and CoTPP/RGO nanocomposite were shown in Fig. 2. The band of RGO at 1628 cm^{-1} was due to the C=C stretching vibration of RGO. The band of CoTPP at 1630 cm^{-1} was due to the C=N stretching vibration of CoTPP. When CoTPP was immobilized on RGO, the $\nu_{C=C}$ and $\nu_{C=N}$ bands of CoTPP/RGO nanocomposite were positively shifted to 1668 cm^{-1}. The positive shift (40 cm^{-1}) can be attributed to the π–π interaction between CoTPP molecule and RGO. It showed that planar RGO could be a good platform for the immobilization of CoTPP molecule.

The morphology of the CoTPP/RGO nanocomposite was characterized by AFM. Fig. 3 showed the AFM images of CoTPP/RGO and RGO. The thickness of RGO was found to be 0.97 nm. In the case of CoTPP/RGO nanocomposite, the thickness increased to 3.6 nm suggesting that CoTPP molecules are adsorbed on the both sides of RGO.

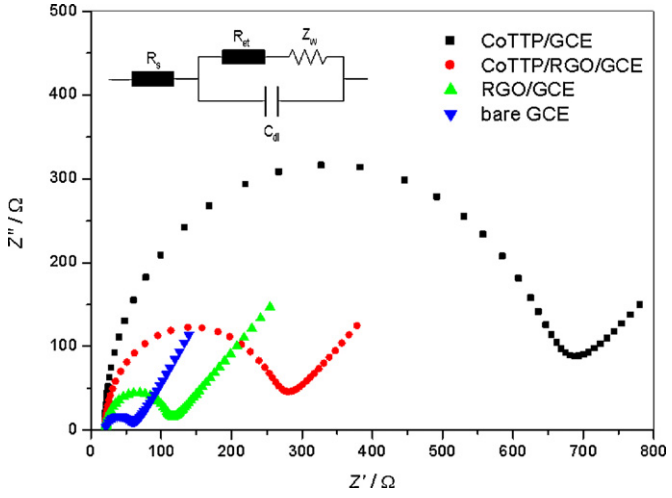

Fig. 4. Electrochemical impedance spectra of bare GCE, RGO/GCE, CoTPP/RGO/GCE and CoTPP/GCE electrodes in 1.0 M KCl + 1.0 mM $K_4Fe(CN)_6/K_3Fe(CN)_6$ aqueous solution.

The conductivity of the CoTPP/RGO nanocomposite was measured by electrochemical impedance spectroscopy (EIS). Fig. 4 compared the impedance spectrum of CoTPP/RGO nanocomposite with that of CoTPP and RGO. The electron-transfer resistance (R_{et})

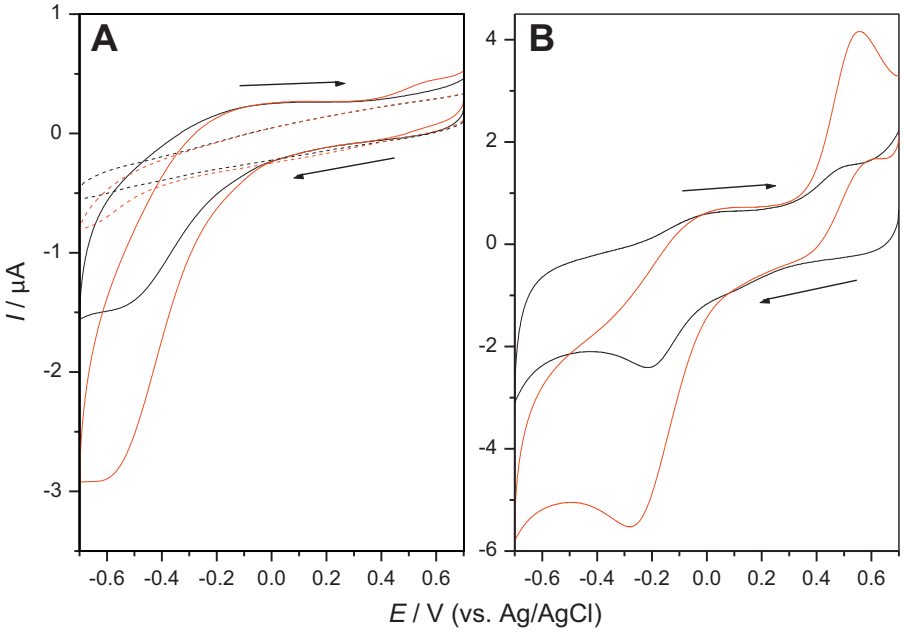

Fig. 5. Cyclic voltammograms of bare GCE (dotted line) and CoTPP/GCE (solid line) (A) and CoTPP/RGO/GCE (B) electrodes in 0.1 M PBS (pH 7.0) in the absence (black line) and presence (red line) of 1.0 mM H_2O_2. Scan rate: 50 mV s^{-1}.

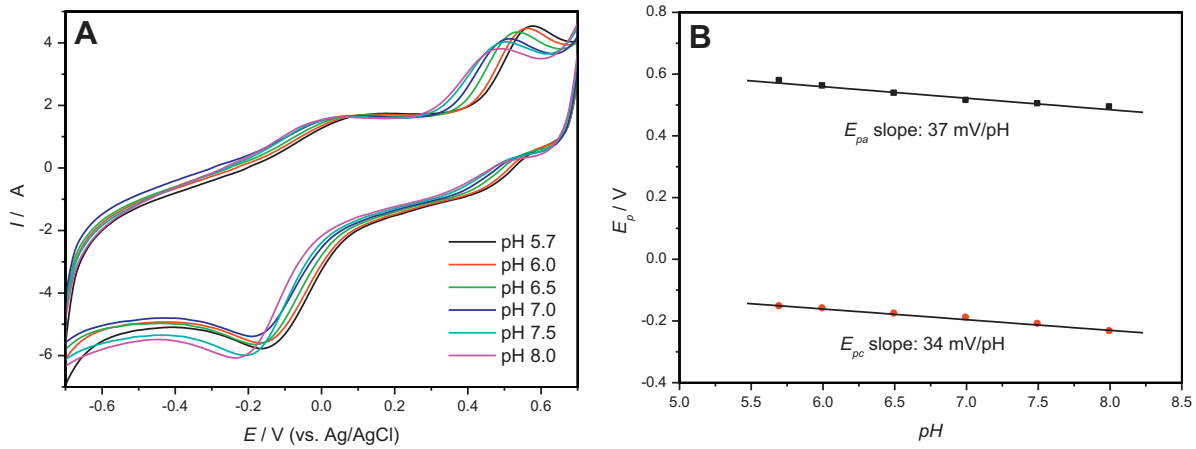

Fig. 6. (A) Cyclic voltammograms of 1.0 mM H_2O_2 at CoTPP/RGO electrode in different pH from 5.7 to 8.0. (B) Dependence of the peak potential on pH.

of CoTPP/RGO nanocomposite was 280 Ω, which was much lower than that of CoTPP (700 Ω). It demonstrated that RGO can promote the electron transfer between CoTPP and electrode surface and the conductivity of CoTPP/RGO nanocomposite was greatly enhanced.

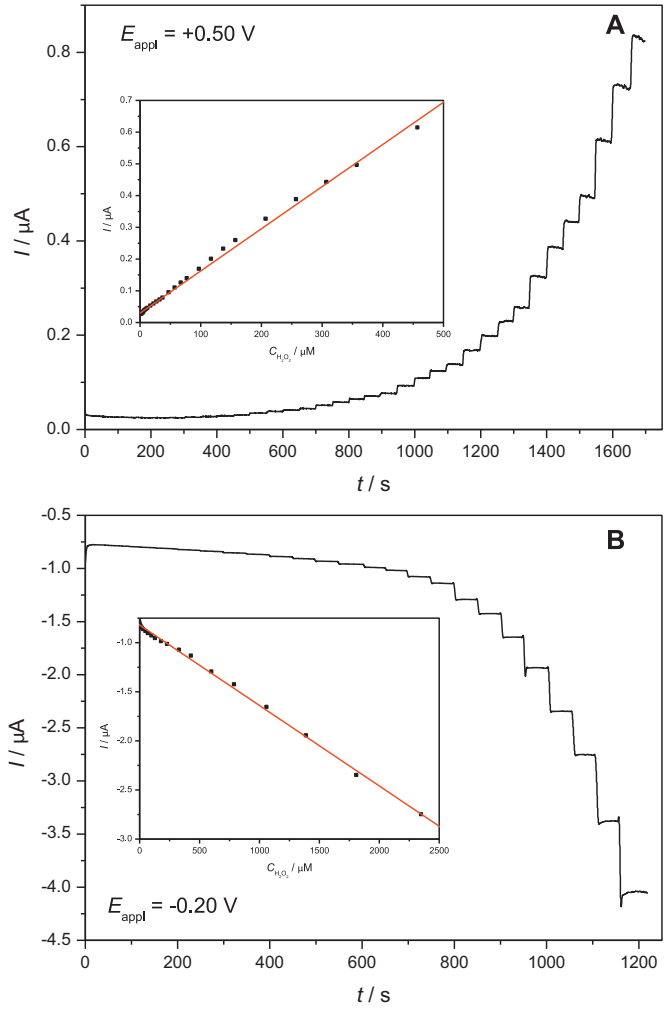

Fig. 7. Chronoamperometric responses of CoTPP/RGO electrode to successive additions of H_2O_2 at the applied potentials of 0.50 V (A) and −0.20 V (B). Insets: the calibration curves of the oxidation current and reduction current on the concentration of H_2O_2.

3.2. Electrocatalysis of H_2O_2 at CoTPP/RGO electrode

Fig. 5 compared cyclic voltammograms of CoTPP/RGO/GCE with those of CoTPP/GCE and bare GCE in the absence and presence of H_2O_2. The electrochemical response of H_2O_2 at the bare GCE is very small and at lower reductive potential of −0.6 V. A large catalytic reduction peak of H_2O_2 at −0.6 V and a small catalytic oxidation peak of H_2O_2 at 0.6 V were observed at CoTPP/GCE electrode. However when CoTPP was adsorbed on the surface of RGO, the catalytic reduction peak potential shifted to −0.25 V, which was 350 mV more positive than that of CoTPP/GCE. And the catalytic oxidation peak potential shifted to 0.55 V, which was 50 mV more negative than that of CoTPP/GCE. The responding reduction current of 1.0 mM H_2O_2 was 3.10 μA, which was 118% higher than that of CoTPP/GCE (1.42 μA). The responding oxidation current of 1.0 mM H_2O_2 was 2.60 μA, which was 25 times higher than that of CoTPP/GCE (0.10 μA). The results indicated that RGO can enhance the electrocatalytic activity of CoTPP and CoTPP/RGO/GCE electrode can electrocatalyze both oxidation and reduction of H_2O_2.

3.3. The mechanism of electrocatalytic oxidation and reduction of H_2O_2 at CoTPP/RGO electrode

The effect of pH on the electrochemical behavior of H_2O_2 at CoTPP/RGO electrode was carefully investigated by cyclic voltammetry in a wide pH range (pH 5.7–8.0) (as shown in Fig. 6). It showed that both the cathodic and anodic peak potentials increased with the increase of pH. Two linear relationships were obtained with the regression equations of E_{pa} (V) = −0.037pH + 0.784 for the H_2O_2 oxidation process and E_{pc} (V) = −0.034pH + 0.0462 for the H_2O_2 reduction process. The slopes of the reduction and the oxidation curves were close to half of the theoretical value of 59 mV pH^{-1}. It indicated that the electrochemical reaction process of H_2O_2 at CoTPP/RGO electrode involved one electron and two protons. The electrode reaction mechanism can be described as follows:

Cathodic reactions:

$$Co(III)TPP + e^- \rightarrow Co(II)TPP$$

$$2Co(II)TPP + 2H^+ + H_2O_2 \rightarrow 2H_2O + 2Co(III)TPP$$

Anodic reactions:

$$Co(III)TPP - e^- + (1/2)H_2O_2 \rightarrow Co(IV)TPP{-}OH$$

$$2Co(IV)TPP{-}OH \rightarrow 2Co(III)TPP + O_2 + 2H^+$$

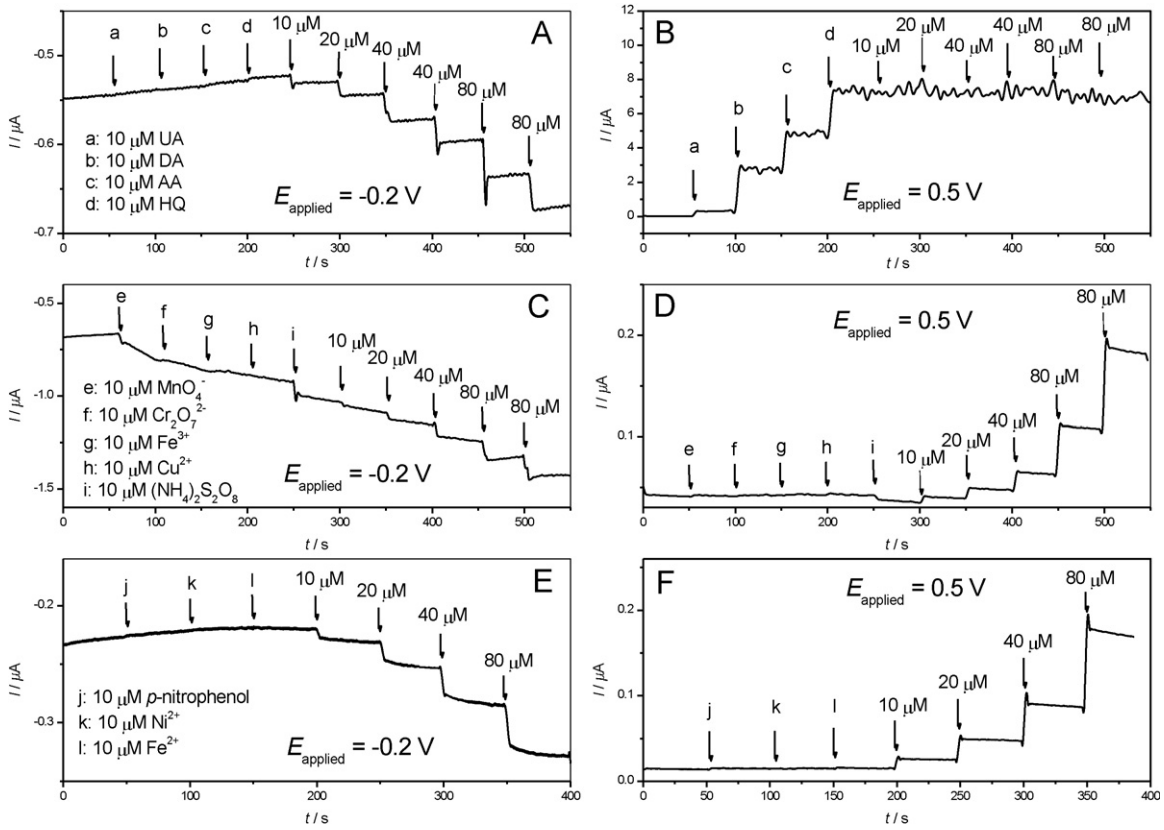

Fig. 8. The amperometric H_2O_2 responses of CoTPP/RGO electrode in the presence of reductive interferences (A and B), oxidative interferences (C and D) and interference species that have both oxidative and reductive activity (E and F) at the applied potential of −0.20 V (A, C, E) and 0.50 V (B, D, F).

3.4. Chronoamperometric responses of H_2O_2 at CoTPP/RGO electrode

Fig. 7A showed steady-state amperometric response of H_2O_2 at CoTPP/RGO electrode at an applied potential of 0.50 V. The response time of the electrode was less than 5 s until steady state value was obtained. The oxidative peak current increased linearly as the H_2O_2 concentration increased. The linear range of H_2O_2 concentration was from 1.0×10^{-7} to 4.6×10^{-4} M with a correlation coefficient of 0.998 and a slope of 0.0013 μA μM^{-1}. The detection limit was 2.0×10^{-8} M at the signal to noise ratio of 3. Fig. 7B showed steady-state amperometric response of H_2O_2 at CoTPP/RGO electrode at an applied potential of −0.20 V. The reductive peak current increased linearly as the H_2O_2 concentration increased. The linear range of H_2O_2 concentration was from 1.0×10^{-7} to 2.4×10^{-3} M with a correlation coefficient of 0.996 and a slope of 0.00082 μA μM^{-1}. The detection limit was 3.2×10^{-8} M at the signal to noise ratio of 3. The high sensitivity of CoTPP/RGO electrode may be due to the synergy effect of CoTPP and RGO in the functional nanocomposite, which accelerate the oxidation of H_2O_2 at lower potential and reduction of H_2O_2 at higher potential.

Table 1 compared the applied potential, linear range, and detection limit of the CoTPP/RGO electrode with those of previously reported enzymatic and non-enzymatic H_2O_2 biosensors [18–25]. The CoTPP/RGO electrode showed wide linear range and low detection limit. Moreover, in this work, both oxidation potential and reduction potential can be applied for the detection of H_2O_2.

Repeated use of the electrodes did not affect the longterm stability. The variation coefficients of the current signals for 8 repeated injections of 10 μM and 40 μM H_2O_2 were 3.5% and 2.8%, respectively. The H_2O_2 biosensor showed good reproducibility with a relative standard deviation of 7.8% at six freshly prepared CoTPP/RGO electrodes. No obvious decrease in the response to H_2O_2 was observed after two months of storage. Therefore, CoTPP/RGO nanocomposite provided an excellent platform for the construction of H_2O_2 biosensor.

3.5. Interference studies at CoTPP/RGO electrode

The effects of foreign interference species on the determination of H_2O_2 at CoTPP/RGO electrode were investigated and presented in Fig. 8. The reductive interferences like UA, DA, AA, HQ, did not affect the measurement of H_2O_2 at the applied potential of −0.2 V (Fig. 8A). However, when the CoTPP/RGO electrode was applied at an oxidative potential of 0.5 V, their interfering effects were severely (Fig. 8B). The oxidative interferences like MnO_4^-, $Cr_2O_7^{2-}$, Fe^{3+}, Cu^{2+}, $(NH_4)_2S_2O_8$ did not affect the measurement of H_2O_2 at the applied potential of 0.5 V (Fig. 8D). However, when the CoTPP/RGO electrode was applied at a reductive potential of −0.2 V, their interfering effects were severely (Fig. 8C). Therefore, excellent interference resistibility of CoTPP/RGO electrode can be achieved at reductive potential of −0.2 V for reductive interference species and at oxidative potential of 0.5 V for oxidative interference species. The interference species which have both oxidative and reductive activity, such as p-nitrophenol, Ni^{2+}, and Fe^{2+} were also investigated (Fig. 8E and F). It showed that they did not affect the measurement of H_2O_2 at both the oxidative potential of 0.50 V and the reductive potential of −0.20 V.

3.6. H_2O_2 testing in real samples

The performance of CoTPP/RGO electrode was compared with that of spectrofluorometry for measuring H_2O_2 in raw whole milk samples. Firstly, 1.8 g $(NH_4)_2SO_4$ was added to 10 mL raw whole

Table 2

Samples	Measured by spectrofluorometer (μM)	Detected (μM)	Added (μM)	Found (μM)	Recovery (%)	R.S.D. (%)
Determination of H_2O_2 in raw whole milk samples at the potential of −0.2 V (n = 3)						
1	8.58	7.96	20	28.35	102.5	3.1
2	7.08	6.75	20	25.97	96.3	2.2
Determination of H_2O_2 in raw whole milk samples at the potential of 0.5 V (n = 3)						
1	8.58	8.25	20	27.89	98.2	1.6
2	7.08	7.17	20	26.94	98.9	2.7

milk with vigorous stirring for 30 min. Then the suspension was centrifuged at 8000 rpm for 10 min, and the supernatant liquid was collected. And then amperometric detection was carried out at the applied potential of −0.2 V and 0.5 V in 10 mL of 0.1 M PBS (pH 7.0) under stirring conditions with 0.5 mL of the supernatant liquid injected. Table 2 summarized the results obtained from the analysis of the two samples by the standard addition method. Compared with the results measured by spectrofluorometer, the results detected by CoTPP/RGO electrode at both −0.2 V and 0.5 V are approximately consistent.

4. Conclusion

In summary, electroactive CoTPP molecules were self-assembled on the surface of two-dimensional RGO by π–π stacking interaction and a novel CoTPP/RGO nanocomposite was formed. The CoTPP/RGO modified electrode exhibited excellent electrocatalytic activity both for oxidation and reduction of H_2O_2. The oxidative peak current was linear to the H_2O_2 concentration with the concentration range from 1.0×10^{-7} to 4.6×10^{-4} M with detection limit of 2.0×10^{-8} M. And the reductive peak current was linear to the H_2O_2 concentration with the concentration range from 1.0×10^{-7} to 2.4×10^{-3} M with detection limit of 3.2×10^{-8} M. The high sensitivity may be due to the synergy effect of CoTPP and RGO in the functional nanocomposite to accelerate the oxidation of H_2O_2 at lower potential and reduction of H_2O_2 at higher potential. At the low oxidative potential of 0.5 V, CoTPP/RGO modified electrode showed good anti-interfering ability towards the oxidative interferences like MnO_4^-, $Cr_2O_7^{2-}$, Fe^{3+}, Cu^{2+}, $(NH_4)_2S_2O_8$. And at the high reductive potential of −0.2 V, CoTPP/RGO modified electrode showed good anti-interfering ability towards the reductive interferences like UA, DA, AA, HQ. The CoTPP/RGO nanocomposite can be a promising electrode material for H_2O_2 biosensor.

Acknowledgements

This work is financially supported by National Science Foundation of China (20965003, 21163007, 21165009, 21210102011), Key Science and Technology Research Program from Ministry of Education of China (210112), and the Scientific Research Foundation for the Returned Overseas Chinese Scholars, State Education Ministry.

References

[1] A. Takai, C.P. Gros, J.M. Barbe, R. Guilard, S. Fukuzumi, Chem. Eur. J. 15 (2009) 3110.
[2] V. Sgobba, G. Giancane, S. Conoci, S. Casilli, G. Ricciardi, D.M. Guldi, M. Prato, L. Valli, J. Am. Chem. Soc. 129 (2007) 3148.
[3] M. Calvete, G.Y. Yang, M. Hanack, Synth. Met. 141 (2004) 231.
[4] R.C. George, T. Mugadza, S. Khene, G.O. Egharevba, T. Nyokong, Electroanalysis 23 (2011) 1699.
[5] W. Zhang, A.U. Shaikh, E.Y. Tsui, T.M. Swager, Chem. Mater. 21 (2009) 3234.
[6] H.P. Li, B. Zhou, Y. Lin, L.R. Gu, W. Wang, K.A.S. Fernando, S. Kumar, L.F. Allard, Y.P. Sun, J. Am. Chem. Soc. 126 (2004) 1014.
[7] G.M.A. Rahman, D.M. Guldi, S. Campidelli, M. Prato, J. Mater. Chem. 16 (2006) 62.
[8] S. Roche, Nat. Nanotechnol. 6 (2011) 8.
[9] Z.L. Wang, D. Xu, Y. Huang, Z. Wu, L.M. Wang, X.B. Zhang, Chem. Commun. 48 (2012) 976.
[10] G.K. Wang, X. Sun, F.Y. Lu, H.T. Sun, M.P. Yu, W.L. Jiang, C.S. Liu, J. Lian, Small 8 (2012) 452.
[11] Z.K. Liu, J.H. Li, Z.H. Sun, G.A. Tai, S.P. Lau, F. Yan, ACS Nano 6 (2012) 810.
[12] Y.X. Xu, L. Zhao, H. Bai, W.J. Hong, C. Li, G.Q. Shi, J. Am. Chem. Soc. 131 (2009) 13490.
[13] Y.F. Xu, Z.B. Liu, X.L. Zhang, Y. Wang, J.G. Tian, Y. Huang, Y.F. Ma, X.Y. Zhang, Y.S. Chen, Adv. Mater. 21 (2009) 1275.
[14] J.X. Geng, H.T. Jung, J. Phys. Chem. C 114 (2010) 8227.
[15] S.Y. Zhang, S. Tang, J.P. Lei, H.F. Dong, H.X. Ju, J. Electroanal. Chem. 656 (2011) 285.
[16] N.I. Kovtyukhova, P.J. Ollivier, B.R. Martin, T.E. Mallouk, S.A. Chizhik, E.V. Buzaneva, A.D. Gorchinskiy, Chem. Mater. 11 (1999) 771.
[17] D. Li, M.B. Muller, S. Gilje, R.B. Kaner, G.G. Wallace, Nat. Nanotechnol. 3 (2008) 101.
[18] M. Shamsipur, M. Asgari, M.F. Mousavi, R. Davarkhah, Electroanalysis 24 (2012) 357.
[19] L. Tian, Y.J. Feng, Y.J. Qi, B.B. Wang, Y.R. Chen, X.Y. Fu, Microchim. Acta 177 (2012) 39.
[20] S.K. Maji, A.K. Dutta, P. Biswas, B. Karmakar, A. Mondal, B. Adhikary, Sens. Actuators B 166 (2012) 726.
[21] L.Q. Luo, F. Li, L.M. Zhu, Z. Zhang, Y.P. Ding, D.M. Deng, Electrochim. Acta 77 (2012) 179.
[22] H.B. Noh, K.S. Lee, P. Chandra, M.S. Won, Y.B. Shim, Electrochim. Acta 61 (2012) 36.
[23] B.J. Wang, L.Q. Luo, Y.P. Ding, D.S. Zhao, Q.L. Zhang, Colloids Surf. B 97 (2012) 51.
[24] X.C. Li, G.H. He, Y. Han, Q. Xue, X.M. Wu, S.R. Yang, J. Colloid Interface Sci. 387 (2012) 39.
[25] Z. Zhang, S.Q. Gu, Y.P. Ding, J.D. Jin, Anal. Chim. Acta 745 (2012) 112.